CrossMark

Structural, spectral, and theoretical investigations of 5-methyl-1-phenyl-1*H*-pyrazole-4-carboxylic acid

Shivapura Viveka[1] · **Gowda Vasantha**[2] ·
Dinesha[1] · **Shivalingegowda Naveen**[3] ·
Neratur Krishnappagowda Lokanath[4] ·
Gundibasappa Karikannar Nagaraja[1]

Abstract The present research work has focused on combined experimental and theoretical studies of one of the biologically important pyrazole-4-carboxylic acid derivatives, viz. 5-methyl-1-phenyl-1*H*-pyrazole-4-carboxylic acid ($C_{11}H_{10}N_2O_2$). The starting material 5-methyl-1-phenyl-1*H*-4-pyrazolecarboxylate (**1**) was obtained by the cyclocondensation of ethyl acetoacetate, *N,N*-dimethylformamide dimethyl acetal (DMF-DMA), and phenylhydrazine, which upon basic hydrolysis yielded the corresponding acid (**2**). The target compound (**2**) was characterized by ^{1}H and ^{13}C NMR (solution in DMSO), Fourier transform infrared (FT-IR) spectroscopy, thermo gravimetric analysis, and by single-crystal X-ray diffraction technique. The single crystals of compound (**2**) were obtained at room temperature by slow evaporation of ethanol as solvent and crystallized in the space group $P2_1/n$ of monoclinic system. The experimental FT-IR and ^{1}H and ^{13}C NMR chemical shifts have been compared to those calculated by means of density functional theory (DFT) at the B3LYP/TZ2P level of theory. The continuum-like screening model was used for geometry optimization of a single molecule and for subsequent cal-

✉ Gundibasappa Karikannar Nagaraja
nagarajagk@gmail.com

1 Department of Studies in Chemistry, Mangalagangotri, Mangalore University, Konaje 574199, India

2 Chemistry of Interfaces, Division of Chemical Engineering, Luleå University of Technology, 97187 Luleå, Sweden

3 Institution of Excellence, Vijnana Bhavana, Manasagangotri, University of Mysore, Mysore 570006, India

4 Department of Studies in Physics, Manasagangotri, University of Mysore, Mysore 570006, India

culations of NMR shielding constants in solution (DMSO). Finally, the HOMO–LUMO energy levels were also constructed to study the electronic transition within the molecule by time-dependent TD-DFT method.

Keywords Pyrazole · Crystallization · FT-IR spectrum · Thermo gram · Crystal structure · NMR · DFT

Introduction

Pyrazoles have been studied for more than a century as an important class of heterocyclic compounds. Pyrazoles are the most important privileged scaffolds found in biologically active molecules and agrochemicals [1]. The pyrazole ring occurs as the core moiety in a variety of leading drugs such as Celebrex, Viagra, and Rimonabant, etc. [8]. Pyrazole, and most of its analogues, have been applied to treat inflammatory [2, 3], diabetic [4], cancer [5], bacterial [6], and analgesic [7] diseases. This class of compounds and its derivatives have been described as useful synthons of various heterocycles and has led to widespread interest in developing new strategies to access these valuable structures. Modification of the structural profile by altering the 1-, 3-, or 4-position substituent in the pyrazole ring affects some bioactivities remarkably [9–11]. The incorporation of acid group into organic molecules, including pyrazole derivatives, has a potential to modify the bioactivities. The presence of this specific functional group opens up a wide range of possibilities for further modification. Moreover, acid functional groups have played a crucial part in the development of theory of heterocyclic compounds, and also they are used extensively in organic synthesis [8, 12–14].

In continuation of our work on the synthesis and discovery of pyrazole derivatives [6, 15, 25–27], herein we describe the synthesis and structural investigations of 5-methyl-1-phenyl-1*H*-pyrazole-4-carboxylic acid (**2**). The compound (**2**) was synthesized by the base hydrolysis of the corresponding ester (**1**) [25]. In our earlier work, we reported the structural analysis of the ester (**1**) by single-crystal X-ray diffraction and thermo-gravimetric analysis (TGA) techniques along with the molecular and electronic structure analysis using DFT methods [15]. In order to comprehend and understand the experimental studies, further theoretical studies need to be carried out aiming to describe the fundamental properties of the present acid.

In order to understand the molecular/electronic structure and properties of pyrazole derivative, we present combined experimental and theoretical investigations of our target acid and the results are compared with our previous work on the corresponding ester [15]. We also present our results on the differential scanning calorimetry (DSC) analysis, which gives information of the heat flow associated with material transition as a function of time and temperature [16], and thermo-gravimetric analysis (TGA), which measures the amount and rate of change in the mass of the sample as a function of temperature [17] of the compound (**2**).

Experimental

Materials and methods

All reagents were purchased from Spectrochem Pvt. Ltd., India, and used without further purification. Infrared spectra was recorded on a Shimadzu FT-IR spectrophotometer in the range of 400–4000 cm^{-1} using the KBr pellets. TGA and DSC were measured using a PerkinElmer Thermal Analysis Instrument and Netzsch Instrument, respectively. Elemental analysis was carried out by using a VARIO EL-III (Elementar 10 Analysensysteme GmBH) instrument. Melting points were determined in open capillary tubes and were uncorrected. The ^{1}H NMR spectra was recorded on a Bruker AV III 400 NMR spectrometer with a 5-mm PABBO BB-1H probe using dimethyl sulfoxide (DMSO-d_6) as solvent. The X-ray intensity data were collected at a temperature of 296 K on a Bruker Proteum2 CCD diffractometer equipped with an X-ray generator operating at 45 kV and 10 mA, using Cu-K$_\alpha$ radiation of wavelength 1.54178 Å. Data were collected for 24 frames per set with different settings of φ (0° and 90°), keeping the scan width of 0.5°, exposure time of 5 s, the sample-to-detector distance of 45.10 mm, and 2θ value at 46.6°. A complete data set was processed using *SAINT PLUS* [18]. The parameters of the molecular geometry, electronic structure, and harmonic frequency calculations were calculated using the Amsterdam Density Functional package (ADF 2014.01) [19, 20]. In all of our calculations, we have used generalized gradient approximation (GGA) with Perdew–Burke–Ernzerhof (PBE) or hybrid B3LYP density functionals [21]. The coordinates from the X-ray diffraction data were used as the starting structure for geometry optimization by DFT method. The geometry was fully optimized at the PBE/TZ2P (triple-ζ basis set with two sets of polarization functions) basis set level followed by the vibrational frequency calculations (no imaginary frequencies). The analytical frequency calculations are fully parallelized and linearly scaled. The ^{1}H and ^{13}C NMR shielding constants and the Frontier molecular orbitals (FMOs) were obtained for the fully optimized monomer of the titled compound at the scalar relativistic ZORA (zeroth-order regular approximation) level of theory using B3LYP/TZ2P methods and the orbitals are plotted using the ADF view program.

Synthesis of 5-methyl-1-phenyl-1*H*-pyrazole-4-carboxylic acid (2)

The synthesis of 5-methyl-1-phenyl-1*H*-pyrazole-4-carboxylate (**1**) is described in our previous report [25]. In the present work (Scheme 1), a mixture of compound (**1**) (1.29 g, 5 mmol) and potassium hydroxide (0.28, 5 mmol) in ethanol (25 ml) was heated under reflux for 5 h and the solvent was distilled in vacuo. The residual mass was poured over crushed ice and neutralized the alkaline solution with 10 % hydrochloric acid. The precipitated crude product was filtered, washed with water, dried, and recrystallized from ethanol to give white crystals of compound (**2**). Yield 1.10 g, (85 %). m.p. 168–170 °C.
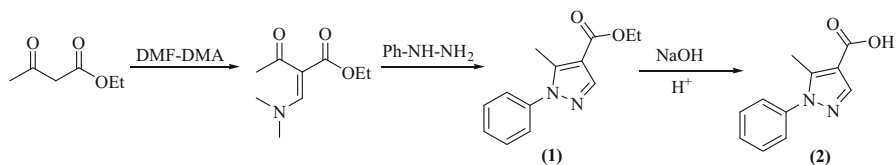
Scheme 1 Proposed reaction scheme for the formation of 5-methyl-1-phenyl-1*H*-pyrazole-4-carboxylic acid (**2**)

Elemental analysis for $C_{11}H_{10}N_2O_2$ (%): C (65.34); H (4.98); N (13.85). Found: C (65.39); H (4.95); N (13.90).

Results and discussions

Thermal analysis (DSC-TGA)

The thermal properties of the 8.07 mg of 5-methyl-1-phenyl-1*H*-pyrazole-4-carboxylic acid (**2**) were investigated in the 25–500 °C temperature range under nitrogen atmosphere at a heating rate of 20 °C/min. The descending TGA thermal curve (Fig. 1) of 8.07 mg of indicates the stages of decomposition at intervals in the
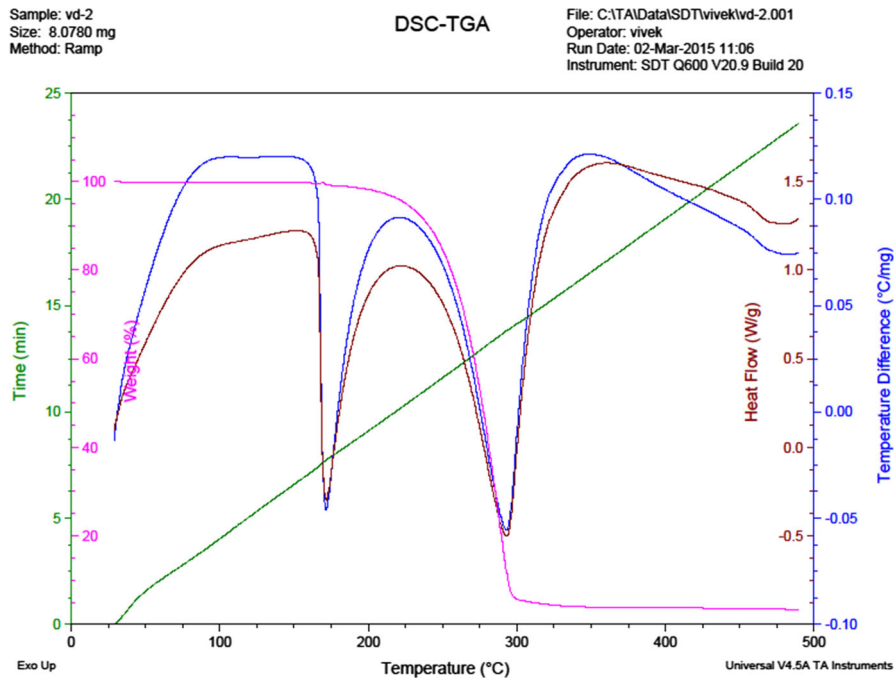

Fig. 1 Thermal analysis of compound **2**

temperature range 20 °C up to 500 °C. The decomposition of the crystal was observed in the temperature range of 220–300 °C. There was no weight loss up to the decomposition temperature, which indicates the absence of moisture in the crystal. The major weight loss that appears in the TGA curve is reflected in the second endothermic peak of the DSC curve. From the DSC curve, the melting point of the material was observed at 171 °C. The sharpness of exothermic peak showed the existence of a good degree of crystallinity and purity of the sample. Further, it indicates that there exists no phase transition before this temperature. Conversion from ester to acid in a 5-methyl-1-phenyl-1*H*-pyrazole increases the thermal stability of the pyrazole (ester decomposes within 271 °C).

^{1}H and ^{13}C NMR spectral analysis

The ^{1}H and ^{13}C NMR spectra of compound (**2**) are shown in Figs. 2 and 3, respectively. In the ^{1}H NMR spectrum, a singlet at δ 2.49 ppm (s, 3H) and the multiplets (m, 5H) in the range of δ 7.48-7.58 ppm can be assigned to methyl and phenyl protons, respectively. The downfield shifted peak at δ 7.96 ppm (s, 1H) can be assigned to the pyrazole proton. The comparatively sharp resonance line for OH proton of the acid at higher δ 12.42 ppm (s, 1H) value is due to the relatively high energy intermolecular H-bonding interactions between acid. The high-resolution ^{13}C NMR spectrum clearly distinguishes all non-equivalent carbons of compound (**2**). For example, the most downfield-shifted resonance line (164.52 ppm) can be assigned to the carboxylic acid carbon without any ambiguity. The resonance lines
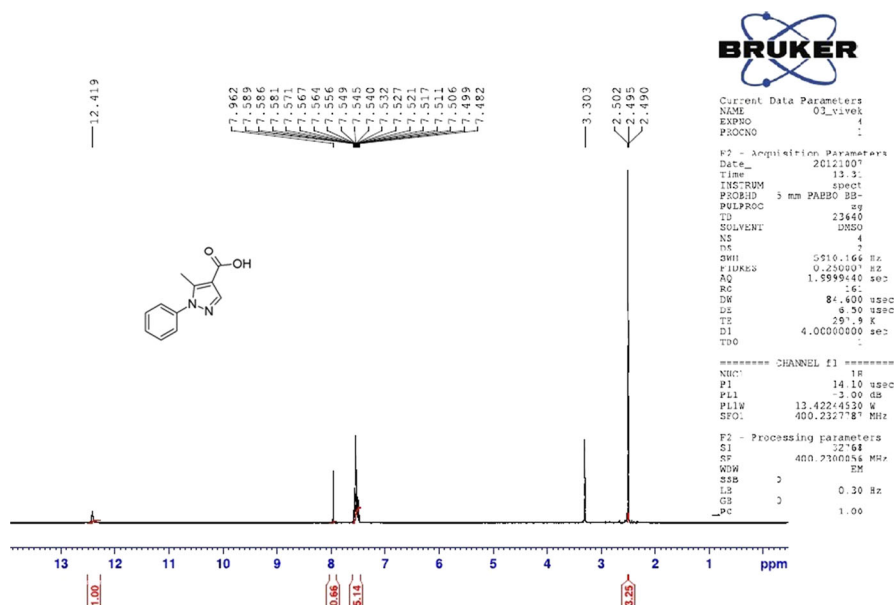

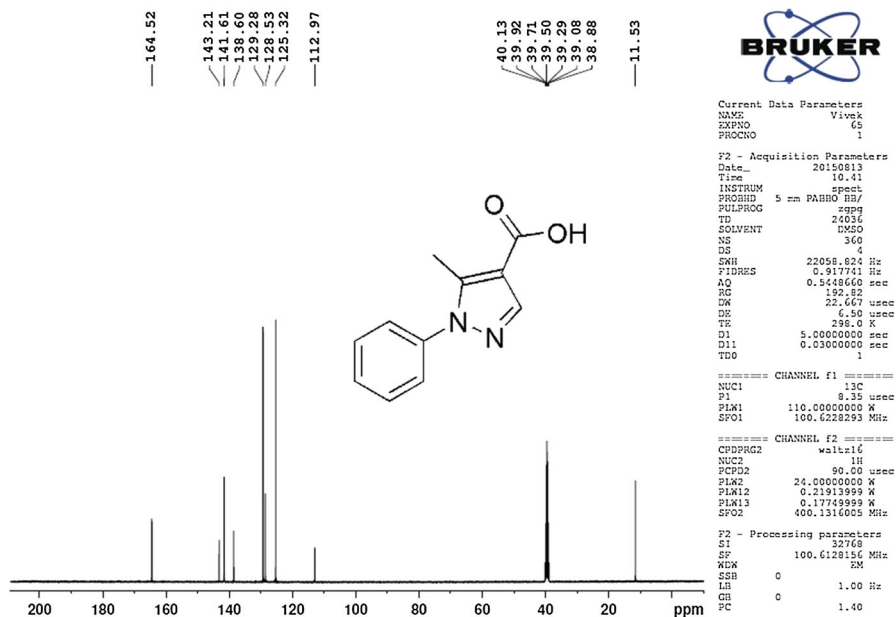**Fig. 2** ^{1}H NMR (400 MHz) spectrum of compound **2** (solution in DMSO)

Fig. 3 ^{13}C NMR (100 MHz) spectrum of compound **2** (solution in DMSO)

in the range of δ 112.97–143.21 ppm are similarly assigned to the sp^2 hybridized carbons. The atom-wise assignment of ^1H and ^{13}C chemical shifts for the titled compound (**2**) is given in Table 1. The regression plot showing the correlation between the calculated and the experimental ^{13}C chemical shift is depicted in Fig. 4. The slope, lower than 1, indicates deviation from the linearity of the calculated values with respect to the experimental results. These discrepancies could be attributed to the fact that there is a strong intermolecular hydrogen bonding between the acids in solution, which was neglected during both the geometry optimization and the NMR chemical shift calculations.

Table 1 Experimental and DFT (B3LYP/TZ2P) calculated ^1H and ^{13}C chemical shifts for title compound (**2**)

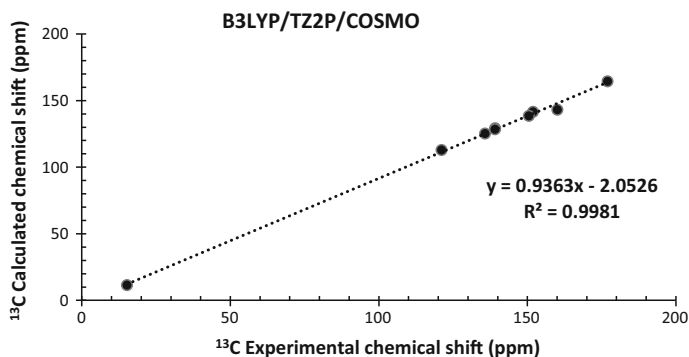| ^{13}C chemical shifts			^1H chemical shifts		
Atoms	Expt.	Calc.	Atoms	Expt.	Calc.
C7	164.52	163.7	–OH	12.44	12.0
C5	143.21	147.8	Py–H	7.96	8.4
C3	141.61	140.2	Ar–H	7.46–7.57	7.8–8.0
C10	138.6	138.9	–CH$_3$	2.49	2.3
C12, C14	129.28	128.2			
C13	128.53	128.2			
C11, C15	125.32	125.0			
C4	112.97	111.3			
C6	11.53	12.2			

Fig. 4 Experimental versus calculated ^{13}C chemical shifts for compound (**2**) in DMSO solution

FT-IR spectral analysis

The theoretical and experimental FT-IR spectrum of compound (**2**) is shown in Fig. 5. The experimental IR vibrational frequencies are assigned as follows (DFT calculated values are within parenthesis).

Pyrazole acid dimers are identified by the bonded O–H stretching absorption at 3419 (3632) cm^{-1}. The band at 2978 (2968–3100) cm^{-1} can be assigned to the symmetric and asymmetric C-H (methyl and phenyl) stretching frequencies of the compound. In addition, due to the monomer–dimer equilibrium, the intramolecular hydrogen bonding resulted in lowering of C=O 1712 (1715) cm^{-1} stretching frequency, which depends upon the degree of hydrogen bonding. The stretching and bending vibrations for pyrazole ring C–C and C–N bonds appeared at 1531 cm^{-1} (1542).

Comparison of the vibrational frequencies calculated at PBE/TZ2P shows reasonably good agreement with experimental values with minor exceptions. For example, the calculated O–H stretching vibration is about 200 cm^{-1} away from the experimental value. Similarly, the vibrational peaks at around 2300 and 1600 cm^{-1} are not seen in the calculated spectrum. These discrepancies between the calculated and experimental vibrational frequencies are because the calculations were performed on a single molecule in the gaseous state unlike the experimental result, which was obtained for the powdered sample and also the molecules are characterized by strong intermolecular interactions. In evidence, the X-ray structure reveals the presence of strong intermolecular hydrogen bonding (O–H⋯O) forming dimers in solid state. On the other hand, the DFT-optimized structure (monomer) has slightly different geometry than the experimental one.

Single-crystal X-ray diffraction

A colorless, rectangular-shaped single crystal of dimensions $0.3 \times 0.27 \times 0.25$ mm of the title compound was chosen for an X-ray diffraction study. The structure was
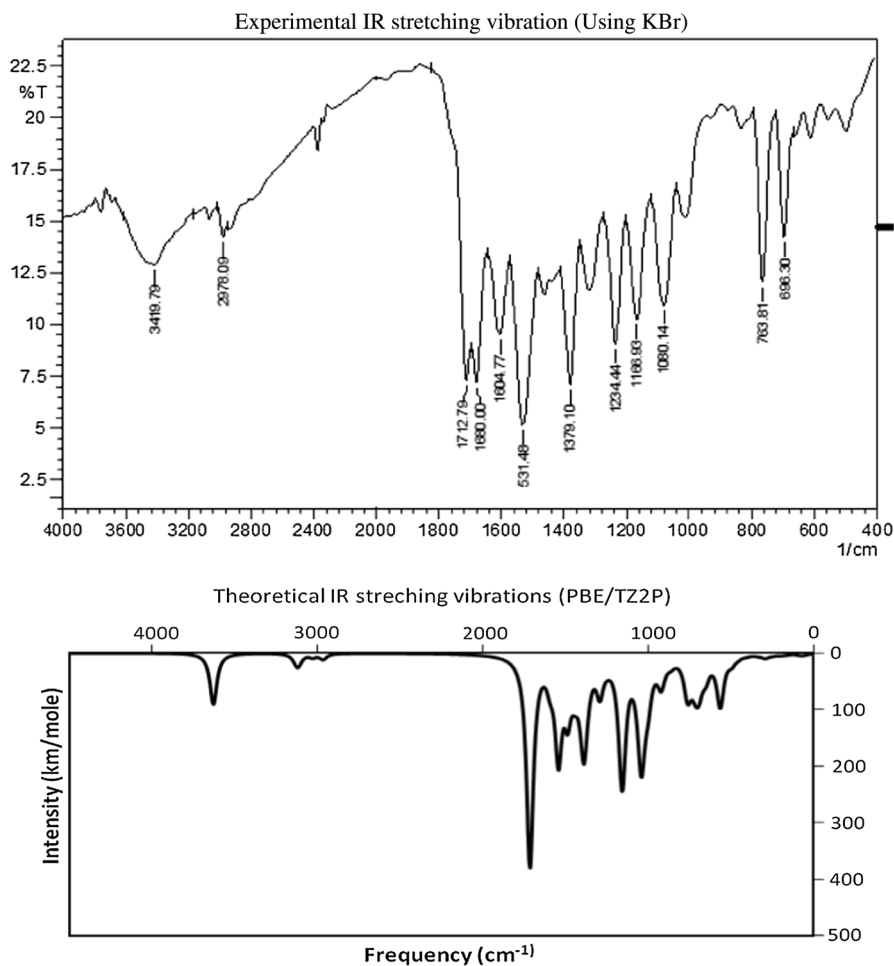
Experimental IR stretching vibration (Using KBr)

Theoretical IR streching vibrations (PBE/TZ2P)

Fig. 5 Experimental (FT-IR spectra using KBr) and theoretical vibrational spectrum (PBE/TZ2P theory level) of the compound **2**

solved by direct methods and refined by full-matrix least-squares method on F^2 using *SHELXS* and *SHELXL* programs [22]. All the non-hydrogen atoms were revealed in the first-difference Fourier map itself. All the hydrogen atoms were positioned geometrically and after several cycles of refinement, the final-difference Fourier map showed peaks of no chemical significance and the residuals saturated to 0.0505. The geometrical calculations were carried out using the program *PLATON* [23]. The molecular and packing diagrams were generated using the software *MERCURY* [24].

The details of the crystal structure and data refinement are given in Table 2. The list of bond lengths and bond angles of the non-hydrogen atoms, together with DFT

calculated values, are given in Tables 3 and 4, respectively. Figure 6 represents the ORTEP diagram of the molecule with thermal ellipsoids drawn at 50 % probability.

A detailed analysis of the molecule shows that all the bond lengths and angles are within the expected ranges. The molecule is non-planar. The bond lengths and bond angles are normal and the molecular conformation is characterized by a dihedral angle of 64.05 (13)°, which is much higher than the reported value of 56.69(10)° for ethyl 5-methyl-1-phenyl-1*H*-pyrazole-4-carboxylate [15]. The carbonyl group at C7 is oriented in a +syn-periplanar conformation as indicated by the torsion angle value of 3.3(4)° for O8–C7–C4–C5, indicating that it lies in the plane of the pyrazole ring.

The crystal structure is stabilized by the intermolecular O–H···O hydrogen bond (O9—H9···O8, 1.81 Å, 165°) (Fig. 7), which links the molecules to form inverted dimers. The packing of the molecules when viewed down along the *c* axis indicates that these inverted dimers run into zig zag chains (Fig. 8).

Table 2 Crystal data and structure refinement table of compound (**2**)

Parameter	Value
CCDC deposit no.	1047065
Empirical formula	$C_{11}H_{10}N_2O_2$
Formula weight	202.21
Temperature	293(2) K
Wavelength	1.54178 Å
Crystal system, space group	Monoclinic, $P2_1/n$
Unit cell dimensions	$a = 5.6872(5)$ Å, $b = 26.979(2)$ Å
	$c = 6.7978(6)$ Å
	$\beta = 105.379(6)°$
Volume	1005.66(15) Å^3
Z, Calculated density	4, 1.336 Mg/m^3
Absorption coefficient	0.775/mm
$F_{(000)}$	424
Crystal size	$0.30 \times 0.27 \times 0.25$ mm
Theta range for data collection	3.28–63.97°
Limiting indices	$-6 \le h \le 5$, $-31 \le k \le 30$, $-7 \le l \le 7$
Reflections collected/unique	7821/1648 [R(int) = 0.0660]
Refinement method	Full-matrix least squares on F^2
Data/restraints/parameters	1648/0/137
Goodness-of-fit on F^2	1.101
Final R indices [$I > 2\sigma(I)$]	$R1 = 0.0505$, $wR2 = 0.1331$
R indices (all data)	$R1 = 0.0678$, $wR2 = 0.1575$
Largest diff. peak and hole	0.166 and -0.228 e Å^{-3}

Table 3 Bond lengths (Å)

Atoms	Length	PBE/TZ2P	Atoms	Length	PBE/TZ2P
N1–C5	1.353(3)	1.373	C7–O8	1.261(3)	1.222
N1–N2	1.375(3)	1.368	C7–O9	1.274(3)	1.371
N1–C10	1.436(3)	1.424	C10–C15	1.375(4)	1.399
N2–C3	1.320(3)	1.324	C10–C11	1.381(3)	1.399
C3–C4	1.401(4)	1.419	C11–C12	1.375(4)	1.395
C4–C5	1.390(3)	1.400	C12–C13	1.381(4)	1.395
C4–C7	1.447(3)	1.459	C13–C14	1.371(4)	1.397
C5–C6	1.484(3)	1.489	C14–C15	1.385(4)	1.393

Table 4 Bond angles (°)

Atoms	Angle	PBE/TZ2P	Atoms	Angle	PBE/TZ2P
C5–N1–N2	113.5(2)	112.8	O8–C7–O9	122.5(2)	121.7
C5–N1–C10	127.8(2)	128.9	O8–C7–C4	120.7(2)	126.4
N2–N1–C10	118.6(2)	118.2	O9–C7–C4	116.8(2)	111.9
C3–N2–N1	103.4(2)	104.7	C15–C10–C11	120.9(2)	120.4
N2–C3–C4	112.5(2)	111.9	C15–C10–N1	119.1(2)	118.8
C5–C4–C3	105.5(2)	105.2	C11–C10–N1	119.9(2)	120.9
C5–C4–C7	127.8(2)	128.0	C12–C11–C10	119.3(2)	119.6
C3–C4–C7	126.4(2)	126.3	C11–C12–C13	120.5(2)	120.2
N1–C5–C4	105.0(2)	105.3	C14–C13–C12	119.6(2)	119.6
N1–C5–C6	122.8(2)	125.0	C13–C14–C15	120.6(3)	120.4
C4–C5–C6	132.1(2)	129.6	C10–C15–C14	119.1(2)	119.7

Gas-phase geometry optimization and electronic structure–property calculations

To compare the structural parameters obtained from the theoretical calculations and the single-crystal X-ray diffraction, we performed geometry optimizations of both the monomeric and dimeric molecules of compound (**2**) (Fig. 9). The analytical frequency calculations on the X-ray diffraction structures (both monomer and dimer) resulted in imaginary frequency values, which is due to the negative vibrational force constants. However, the fully optimized structures resulted all vibrational force constants positive and no imaginary frequency has appeared. In other words, the optimized structures were sitting at a true minimum at the potential energy surface. The theoretical bond lengths and bond angles for the monomer are given in Tables 3 and 4 together with the experimental values. The experimental bond parameters were well reproduced by the calculations with few exceptions. The
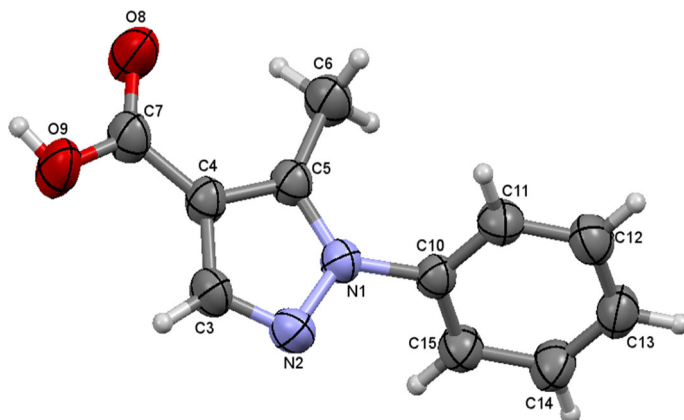
Fig. 6 ORTEP of the molecule with thermal ellipsoids drawn at 50 % probability
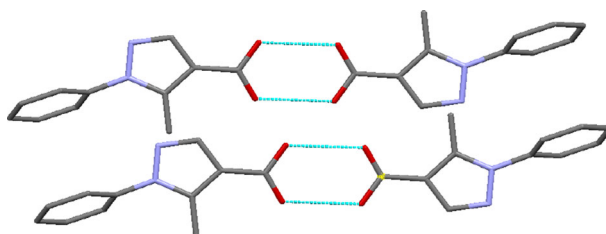

Fig. 7 A view of the crystal packing of the title compound showing inverted dimers

bond lengths were overestimated by ca 0.01 Å for all phenyl C–C bonds whereas the variations of bond angles were all uneven. The largest deviations were observed for C–O bond length (0.1 Å) and O–C–C bond angles (4°–6°).

TD-DFT calculations

In order to study the characteristics of electronic transition and oscillator strength (*F*) of compound (**2**), a single-point, time-dependent DFT calculation of lowest singlet–singlet transitions were performed by employing the B3LYP functional at scalar-relativistic ZORA level. The results are listed in Table 5.

Figure 10 lists the energies and percentage composition of few FMOs viz. LUMO+1, LUMO, HOMO, and HOMO−1, calculated using PBE and B3LYP density functionals. It is a known fact that pure GGA functionals such as PBE generally underestimate the band gap. The calculated energy difference between HOMO and LUMO for the title complex is 4.18 eV (PBE) and 5.48 eV (B3LYP). The HOMO is mostly composed of both phenyl and pyrazole carbons as well as the pyrazole nitrogens with small contributions from the oxygen atoms whereas the LUMO is almost spread over the entire molecule. The two major electronic transitions for the compound exhibiting a large oscillator strength and assigned to
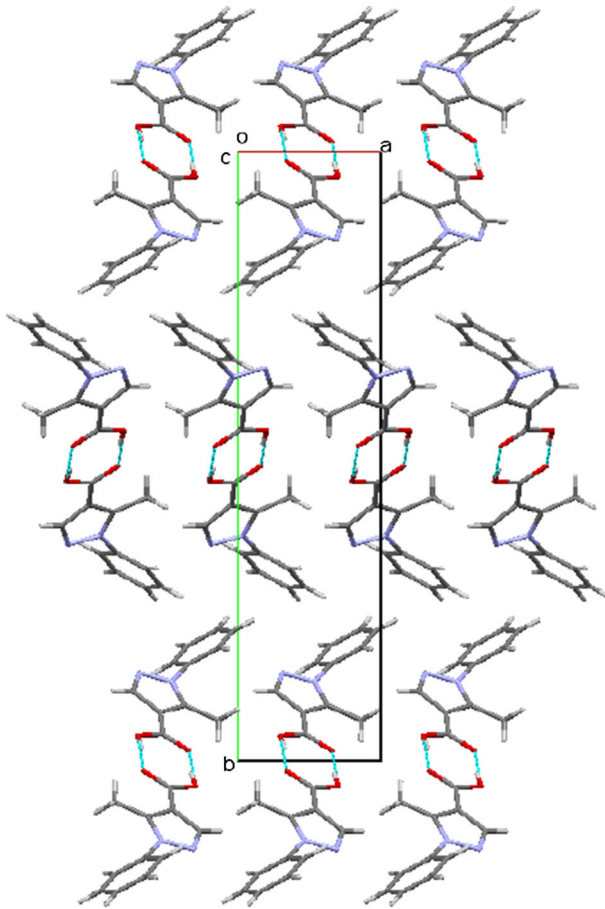
Fig. 8 Packing of the molecules when viewed along the *c* axis. The *dotted lines* represent inter-molecular hydrogen bonds linking the molecules into zig zag chains
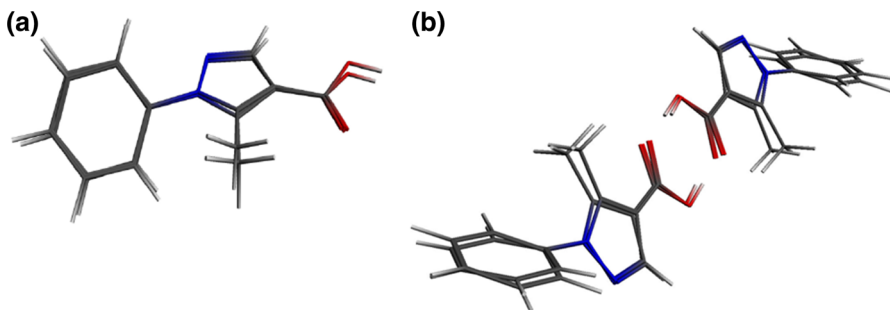

Fig. 9 The DFT optimized structure overlaid with monomer of the X-ray diffraction structure (PBE/TZ2P level of theory)

Table 5 TD-DFT calculation of excitation energies (E) and oscillator strength (F) of the lowest excited singlet–singlet states

TD-DFT state	E/a.u.	E/eV	F
S_0	0.18153	4.93979	0.410400
S_1	0.18484	5.02965	0.003989
S_2	0.18854	5.13031	0.002504
S_3	0.19277	5.24552	0.033990
S_4	0.20548	5.59127	0.000107
S_5	0.20723	5.63888	0.039050
S_6	0.21196	5.76760	0.106900
S_7	0.21235	5.77835	0.172400
S_8	0.21980	5.98108	0.000239
S_9	0.22574	6.14278	0.032760
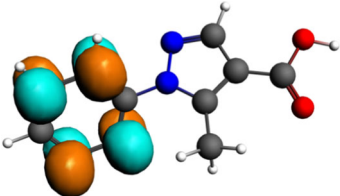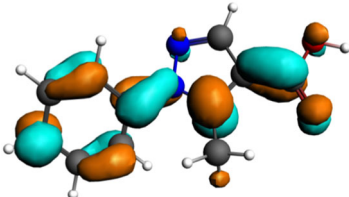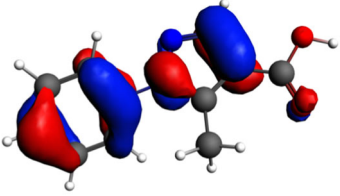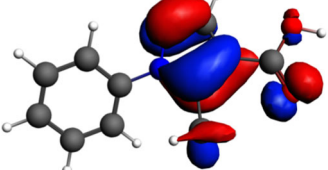
Orbitals	Frontier molecular orbitals (FMOs)	Energy	C%	N%	O%
LUMO+1		-1.774 (-0.947)	92.1 (90.4)	-	-
LUMO		-2.249 (-1.478)	77.1 (76.2)	4.6 (5.8)	8.5 (7.6)
HOMO		-6.266 (-6.925)	74.7 (72.8)	16.4 (15.3)	2.3 (1.3)
HOMO-1		-6.428 (-7.221)	40.5 (50.4)	26.9 (31.6)	16.8 (4.8)

Fig. 10 Frontier molecular orbital (FMO) analysis, energies, and percent atomic contribution to the frontier molecular orbitals of the title compound at the PBE and B3LYP (*within parenthesis*) scalar relativistic ZORA level with TZ2P basis set

S_0–S_1, which corresponds essentially to the HOMO–LUMO, HOMO−1−LUMO, HOMO–LUMO+1, HOMO–LUMO+2, HOMO−2−LUMO excitations. HOMO−1 shows orbital contributions from the pyrazole ring alone whereas LUMO + 1 is composed of orbitals of phenyl ring (except C8 and C11). The HOMOs are generally of bonding character, while the LUMOs are mostly antibonding in nature and essentially delocalized over the entire molecule.

Conclusions

The present study reports the successful synthesis and single-crystal X-ray diffraction analysis of 5-methyl-1-phenyl-1*H*-pyrazole-4-carboxylic acid. The titled compound was crystallized in the space group *P*2$_1$/*n* of monoclinic system and structure was stabilized by the intermolecular O–H···O hydrogen bond. The DFT-based ^{1}H and ^{13}C NMR chemical shift calculations were in good agreement with the experimental results. The assignments of most of the fundamental vibrational modes of the title compound were made based on the results of the DFT calculations. Both HOMO and LUMO is delocalized over the phenyl and pyrazole group with small contributions from the oxygen atoms whereas the HOMO−1 and LUMO+1 are composed of either phenyl or pyrazole groups, respectively. All the experimental results are successfully compared with our previous reports of 5-methyl-1-phenyl-1*H*-4-pyrazolecarboxylate.

References

1. S. Fustero, M. Sanchez-Rosello, P. Barrio, A. Simon-Fuentes, Chem. Rev. **111**, 6984–7034 (2011)
2. A.A. Bekhit, A. Hymete, A.A. Bekhit, A.D. Mamuye, H.Y. Aboul-Enein, Rev. Med. Chem. **10**, 1014–1033 (2010)
3. L. Nagarapu, J. Mateti, H.K. Gaikwad, R. Bantu, M. Sheeba, Rani, N.J. Prameela Subhashini. Bioorg. Med. Chem. Lett. **21**, 4138–4140 (2011)
4. F.F. Noe, L. Fowden, Nature **184**, 69–70 (1959)
5. S.L. Zhu, Y. Wu, C.-J. Liu, C.-J. Wei, J.-C. Tao, H.-M. Liu, Eur. J. Med. Chem. **65**, 70–82 (2013)
6. S. Viveka, Dinesha, L.N. Madhu, G.K. Nagaraja, Monatsh. Chem. **146**, 1547–1555 (2015)
7. A.M. Vijesh, A.M. Isloor, P. Shetty, S. Sundershan, H.K. Fun, Eur. J. Med. Chem. **62**, 410–415 (2013)
8. S. Mert, R. Kasımoğulları, T. İça, F. Çolak, A. Altun, S. Ok, Eur. J. Med. Chem. **78**, 86–96 (2014)
9. B. Çalışkan, A. Yılmaz, I. Evren, S. Menevşe, O. Uludag, E. Banoglu, Med. Chem. Res. **22**, 782–793 (2013)
10. T. Dey, J. Jacob, S. Sahu, M. Baidya, Pharmacologyonline **1**, 908–916 (2011)
11. P. Khloya, P. Kumar, A. Mittal, N.K. Aggarwal, P.K. Sharma, Org. Med. Chem. Lett. **3**, 9 (2013)
12. Ş.C. Pirol, B. Çalışkan, İ. Durmaz, R. Atalay, E. Banoglu, Eur. J. Med. Chem. **87**, 140–149 (2014)
13. O. Bruno, C. Brullo, F. Bondavalli, S. Schenone, S. Spisani, M.S. Falzarano, K. Varani, E. Barocelli, V. Ballabeni, C. Giorgio, M. Tognolini, Bioorg. Med. Chem. **17**, 3379–3387 (2009)
14. L.-L. Xu, C.-J. Zheng, L.-P. Sun, J. Miao, H.-R. Piao, Eur. J. Med. Chem. **48**, 174–178 (2012)

15. S. Viveka, G. Vasantha, Dinesha, S. Naveen, N.K. Lokanath, G.K. Nagaraja, Mol. Cryst. Liq. Cryst. (Accepted May 2015)
16. Y.-H. Luo, B.-W. Sun, Spectrochim. Acta Part A. **120**, 381–388 (2014)
17. S. Viveka, M. Prabhuswamy, Dinesha, N.K. Lokanath, G.K. Nagaraja, Mol. Cryst. Liq. Cryst. **593**, 261–270 (2014)
18. Bruker. SAINT PLUS, Bruker AXS Inc. Madison, Wisconsin, USA (2012)
19. G. te Velde, F.M. Bickelhaupt, S.J.A. van Gisbergen, C.F. Guerra, E.J. Baerends, J.G. Snijders, T. Ziegler, J. Comput. Chem. **22**, 931–967 (2001)
20. GUI. SCM, Amsterdam, The Netherlands, http://www.scm.com (2014)
21. J.P. Perdew, K. Burke, M. Ernzerhof, Phys. Rev. Lett. **77**, 3865–3868 (1996)
22. G.M. Sheldrick, Acta Cryst. **A64**, 112–122 (2008)
23. A.L. Spek, Acta. Cryst. **A46**, C34 (1990)
24. C.F. Macrae, I.J. Bruno, J.A. Chisholm, P.R. Edgington, P. McCabe, E. Pidcock, L. Rodriguez-Monge, R. Taylor, J. van de Streek, P.A. Wood, J. Appl. Cryst. **41**, 466–470 (2008)
25. S. Viveka, Dinesha, P. Shama, G.K. Nagaraja, N. Deepa, M.Y. Sreenivasa, Res. Chem. Intermed. (2015) (Accepted)
26. S. Viveka, Dinesha, P. Shama, G.K. Nagaraja, S. Ballav, S. Kerkar, Eur. J. Med. Chem. **101**, 442–451 (2015)
27. S. Viveka, Dinesha, S.S. Laxmeshwar, G.K. Nagaraja, Molbank. **3**, M776 (2012)